Cosmological constraints on post-Newtonian parameters in effectively massless scalar-tensor theories of gravity

Massimo Rossi,[1,*] Mario Ballardini,[2,3,1,†] Matteo Braglia,[4,1,5,‡] Fabio Finelli,[1,5,§] Daniela Paoletti,[1,5,¶] Alexei A. Starobinsky,[6,7,**] and Caterina Umiltà[8,††]

[1] *INAF/OAS Bologna, via Gobetti 101, I-40129 Bologna, Italy*
[2] *Dipartimento di Fisica e Astronomia, Alma Mater Studiorum Universitá di Bologna, Via Gobetti, 93/2, I-40129 Bologna, Italy*
[3] *Department of Physics and Astronomy, University of the Western Cape, Cape Town 7535, South Africa*
[4] *Dipartimento di Fisica e Astronomia, Alma Mater Studiorum, Università degli Studi di Bologna, via Gobetti 101, I-40129 Bologna, Italy*
[5] *INFN, Sezione di Bologna, Via Irnerio 46, I-40127 Bologna, Italy*
[6] *Landau Institute for Theoretical Physics, 119334 Moscow, Russia*
[7] *Bogolyubov Laboratory of Theoretical Physics, Joint Institute for Nuclear Research, Dubna 141980, Russia*
[8] *Department of Physics, University of Cincinnati, 345 Clifton Ct, Cincinnati, OH 45221, U.S.A.*

(Dated: February 7, 2020)

We study the cosmological constraints on the variation of the Newton's constant and on post-Newtonian parameters for simple models of scalar-tensor theory of gravity beyond the extended Jordan-Brans-Dicke theory. We restrict ourselves to an effectively massless scalar field with a potential $V \propto F^2$, where $F(\sigma) = N_{pl}^2 + \xi\sigma^2$ is the coupling to the Ricci scalar considered. We derive the theoretical predictions for cosmic microwave background (CMB) anisotropies and matter power spectra by requiring that the effective gravitational strength at present is compatible with the one measured in a Cavendish-like experiment and by assuming adiabatic initial condition for scalar fluctuations. When comparing these models with *Planck* 2015 and a compilation of baryonic acoustic oscillations data, all these models accomodate a marginalized value for H_0 higher than in ΛCDM. We find no evidence for a statistically significant deviation from Einstein's general relativity. We find $\xi < 0.064$ ($|\xi| < 0.011$) at 95% CL for $\xi > 0$ (for $\xi < 0$, $\xi \neq -1/6$). In terms of post-Newtonian parameters, we find $0.995 < \gamma_{\rm PN} < 1$ and $0.99987 < \beta_{\rm PN} < 1$ ($0.997 < \gamma_{\rm PN} < 1$ and $1 < \beta_{\rm PN} < 1.000011$) for $\xi > 0$ (for $\xi < 0$). For the particular case of the conformal coupling, i.e. $\xi = -1/6$, we find constraints on the post-Newtonian parameters of similar precision to those within the Solar System.

I. INTRODUCTION

The astrophysical and cosmic tests for the change of the fundamental physical constants are improving thanks to the increasing precision of observations [1, 2]. In most of the cases these tests cannot compete with the precision which can be achieved in laboratories, but can probe lengths and/or timescales otherwise unaccessible on ground. There are however exceptions: for instance, current cosmological data can constrain the time variation of the Newtonian constant at the same level of experiments within the Solar System such as the Lunar Laser ranging [3, 4].

As far as cosmological tests are concerned, one of workhorse model to test deviations from general relativity (GR) is the extended Jordan-Brans-Dicke (eJBD) [5, 6] theory, which has been extensively studied [3, 4, 7–12]. eJBD is perhaps the simplest extension of GR within the more general Horndeski theory [13]:

$$S = \int \mathrm{d}^4x\sqrt{-g}\Big[G_2(\sigma,\chi) + G_3(\sigma,\chi)\Box\sigma + G_4(\sigma,\chi)\,R - 2G_{4,\chi}(\sigma,\chi)\left(\Box\sigma^2 - \sigma^{;\mu\nu}\sigma_{;\mu\nu}\right) + G_5(\sigma,\chi)G_{\mu\nu}\sigma^{;\mu\nu} + \frac{1}{3}G_{5,\sigma}(\sigma,\chi)\left(\Box\sigma^3 - 3\sigma_{;\mu\nu}\sigma^{;\mu\nu}\Box\sigma + 2\sigma_{;\mu\nu}\sigma^{;\nu\rho}\sigma^{;\mu}{}_{;\rho}\right) + \mathcal{L}_m\Big], \quad (1)$$

where $\chi = -g^{\mu\nu}\partial_\mu\sigma\partial_\nu\sigma$, "$;$" denotes the covariant derivative, R is the Ricci scalar, $G_{\mu\nu} = R_{\mu\nu} - g_{\mu\nu}R/2$, and $\mathcal{L}_m$ is the density Lagrangian for the rest of matter. The eJBD theory corresponds to $G_3 = G_5 = 0$, $G_2 = \omega_{\rm BD}\chi/\sigma - V(\sigma)$, $G_4 = \sigma$ (in the equivalent induced gravity (IG) formulation with a standard kinetic term the two last conditions become $G_2 = \chi/2 - V(\sigma)$, $G_4 = \xi\sigma^2/2$ with $\xi = 1/(4\omega_{\rm BD})$).

Cosmology puts severe test on eJBD theories. The constraints from *Planck* 2015 and a compilation of baryon acoustic oscillations (BAO) data lead to a 95% CL upper bound $\xi < 0.00075$, weakly dependent on the index for a power-law potential [4] (see [3] for the *Planck* 2013 constraints obtained with the same methodology). In terms of the first post-Newtonian parameter $\gamma_{\rm PN} = (1+\omega_{\rm BD})/(2+\omega_{\rm BD}) = (1+4\xi)/(1+8\xi)$, the above 95% CL constraint read as $|\gamma_{\rm PN} - 1| < 0.003$ [4]. With the same data, a 95% CL bound is obtained on the rel-

* rossi.massim@gmail.com
† mario.ballardini@inaf.it
‡ matteo.braglia2@unibo.it
§ fabio.finelli@inaf.it
¶ daniela.paoletti@inaf.it
** alstar@landau.ac.ru
†† umiltca@ucmail.uc.edu

ative time variation of the effective Newton's constant $10^{13}|\dot{G}_{\rm eff}/G_{\rm eff}| \lesssim 6\times10^{-3}\ H_0$ at 95% CL with an index for a power-law potential in the range $[0,8]$. The combination of future measurement of CMB anisotropies in temperature, polarization and lensing with Euclid-like (galaxy clustering and weak lensing) data can lead to constraints on $\gamma_{\rm PN}$ at a slightly larger level than the current Solar System constraints [14] (see also [15] for forecasts for different experiments with different assumptions).

However, theoretical priors can play an important role in the derivation of the cosmological constraints and need to be taken into account in the comparison with other astrophysical or laboratory tests. Indeed, for eJBD theories only the first post-Newtonian parameter $\gamma_{\rm PN}$ is nonzero and fully encodes the deviations from GR, being the second post-Newtonian parameter $\beta_{\rm PN}\propto {\rm d}\gamma_{\rm PN}/{\rm d}\sigma$. In this paper we wish to go beyond the working assumption of $\beta_{\rm PN}=0$ implicit within in eJBD theories. For this purpose we therefore consider nonminimally coupled (NMC) scalar fields with $2G_4=N_{\rm pl}^2+\xi\sigma^2$ as a minimal generalization of the eJBD theories. NMC with this type of coupling are also known as extended quintessence models in the context of dark energy [16–20]. As for eJBD, NMC are also within the class of Horndeski theories consistent with the constraints on the velocity of propagation of gravitational waves [21–23] which followed the observation of GW170817 and its electromagnetic counterpart [24] (see also [25, 26]).

The outline of this paper is as follows. In Section II we discuss the background dynamics and the post-Newtonian parameters $\gamma_{\rm PN}$ and $\beta_{\rm PN}$ for this class of scalar-tensor theories. We study the evolution of linear fluctuations in Section III. We show the dependence on ξ of the CMB anisotropies power spectra in temperature and polarization in Section IV. We present the *Planck* and BAO constraints on these models in Section V. We conclude in Section VI. The initial conditions for background and cosmological fluctuations are collected in Appendix A.

II. DARK ENERGY AS AN EFFECTIVELY MASSLESS SCALAR FIELD NON-MINIMALLY COUPLED TO GRAVITY

We study the restriction of the Horndeski action (1) to a standard kinetic term and $G_3=G_5=0$. We also assume:

$$2G_4\equiv F(\sigma)=N_{\rm pl}^2+\xi\sigma^2\,, \tag{2}$$

where ξ is the coupling to the Ricci scalar which is commonly used in extended quintessence [16–20]. For simplicity we denote by a tilde the quantities normalized to $M_{pl}\equiv 1/\sqrt{8\pi G}$, where $G=6.67\times10^{-8}$ cm^3 g^{-1} s^{-2} is the gravitational constant measured in a Cavendish-like experiment. We also introduce the notation $\tilde{N}_{pl}\equiv 1\mp\Delta\tilde{N}_{pl}$ for $\xi\gtrless 0$.

The field equations are obtained by varying the action with respect to the metric:

$$\begin{aligned}G_{\mu\nu}=\frac{1}{F(\sigma)}\Big[&T_{\mu\nu}+\partial_\mu\sigma\partial_\nu\sigma-\frac{1}{2}g_{\mu\nu}\partial^\rho\sigma\partial_\rho\sigma\\&-g_{\mu\nu}V(\sigma)+(\nabla_\mu\nabla_\nu-g_{\mu\nu}\Box)F(\sigma)\Big]\,.\end{aligned} \tag{3}$$

The Einstein trace equation results:

$$R=\frac{1}{F}\left[-T+\partial_\mu\sigma\partial^\mu\sigma+4V+3\Box F\right], \tag{4}$$

where T is the trace of the energy-momentum tensor. The Klein-Gordon (KG) equation can be obtained varying the action with respect to the scalar field:

$$-\Box\sigma-\frac{1}{2}F_{,\sigma}R+V_{,\sigma}=0, \tag{5}$$

and substituting the Einstein trace equation one obtains:

$$\begin{aligned}&-\Box\sigma\left(1+\frac{3}{2}\frac{F_{,\sigma}^2}{F}\right)+V_{,\sigma}-2\frac{VF_{,\sigma}}{F}\\&+\frac{F_{,\sigma}}{2F}\left[T-\partial_\mu\sigma\partial^\mu\sigma\left(1+3F_{,\sigma\sigma}\right)\right]=0\,.\end{aligned} \tag{6}$$

In this paper, we do not consider a quintessence-like inverse power-law potential (see for instance [16–18, 20]), but we restrict ourselves to a potential of the type $V\propto F^2$ in which the scalar field is effectively massless. This case generalizes the broken scale invariant case [27–29] to NMC and is a particular case of the class of models with $V\propto F^M$ admitting scaling solutions [19]. Note that though for the form of $F(\sigma)$ used in the paper and for large values of σ, this potential looks similar to that in the Higgs inflationary model [30], in fact it is crucially different, since it is exactly flat in the Einstein frame* in the absence of other matter and cannot support a metastable inflationary stage in the early Universe. Contrary, this model may be used for description of dark energy in the present Universe.

A. Background cosmology

We consider cosmic time and a flat FLRW metric, for which the unperturbed cosmological spacetime metric is given by:

$${\rm d}s^2=-{\rm d}t^2+a(t)^2{\rm d}x_i{\rm d}x^i. \tag{7}$$

* Although our work is based in the original Jordan frame, it is also useful to think about this class of theories in the dual Einstein frame where $\hat{g}_{\mu\nu}\propto Fg_{\mu\nu}\,,\hat{V}=V/F^2$.

The Friedmann and the KG equations are then given by:

$$
\begin{aligned}
3H^2F &= \rho + \frac{\dot\sigma^2}{2} + V(\sigma) - 3H\dot F && (8)\\
&= \rho + \rho_\sigma, && (9)\\
-2\dot H F &= \rho + p + \dot\sigma^2 + \ddot F - H\dot F && (10)\\
&= (\rho + p) + \rho_\sigma + p_\sigma. && (11)
\end{aligned}
$$

$$
\begin{aligned}
\ddot\sigma = &-3H\dot\sigma + \frac{\xi\sigma}{F + 6\xi^2\sigma^2}\Big[\rho_m + 4V - \frac{FV_{,\sigma}}{\xi\sigma} \\
&- (1+6\xi)\dot\sigma^2\Big].
\end{aligned} \qquad (12)
$$

In Fig. 1 the evolution of the scalar field σ is shown for different values of ξ for both positive and negative values of the coupling. The natural initial conditions for the background displayed in Appendix A neglect the decaying mode which would be rapidly dissipated, but would have destroyed the Universe isotropy at sufficiently early times otherwise (see for instance [29]). With this natural assumption the scalar field is nearly at rest deep in the radiation era whereas it grows (decreases) for positive (negative) couplings during the matter era and it reaches a constant value at recent times. During the matter dominated era in the regime $\xi\sigma^2 \ll N_{\rm pl}^2$ (which is the only one allowed by observations, see Section V), the evolution of the scalar field can be approximated as $\sigma \sim \sigma_i\,[1 + 2\xi(\ln a + 8)]$, with σ_i being the initial value of the scalar field in the radiation era. In the bottom panel, we show the evolution of the scalar field for the conformal coupling (CC) case with $\xi = -1/6$ for different values of $N_{\rm pl}$. In this case the field is always sub-Planckian for $\Delta\tilde N_{\rm pl} \lesssim 0.0005$.

The above equations lead to the straightforward associations:

$$
\begin{aligned}
\rho_\sigma &= \frac{\dot\sigma^2}{2} + V(\sigma) - 3H\dot F \\
&= \frac{\dot\sigma^2}{2} + V(\sigma) - 6H\xi\sigma\dot\sigma,
\end{aligned} \qquad (13)
$$

$$
\begin{aligned}
p_\sigma = &\frac{\dot\sigma^2}{2}\left[\frac{F(1+4\xi) + 2\xi^2\sigma^2}{F + 6\xi^2\sigma^2}\right] - 2H\xi\sigma\dot\sigma \\
&+ \frac{2\xi^2\sigma^2}{F + 6\xi^2\sigma^2}\left(\rho_m + 4V - \frac{FV_{,\sigma}}{\xi\sigma}\right) - V,
\end{aligned} \qquad (14)
$$

where in the equation for p_σ we have explicitly substituted the KG equation. We can recover an expression for the dark energy (DE) density parameter dividing ρ_σ for the quantity $3H^2F$ which represents the critical density.

Alternatively, it is also convenient to define new density parameters in a framework which mimics Einstein gravity at present and satisfy the conservation law $\dot\rho_{\rm DE} + 3H(\rho_{\rm DE} + p_{\rm DE}) = 0$ [31, 32]:

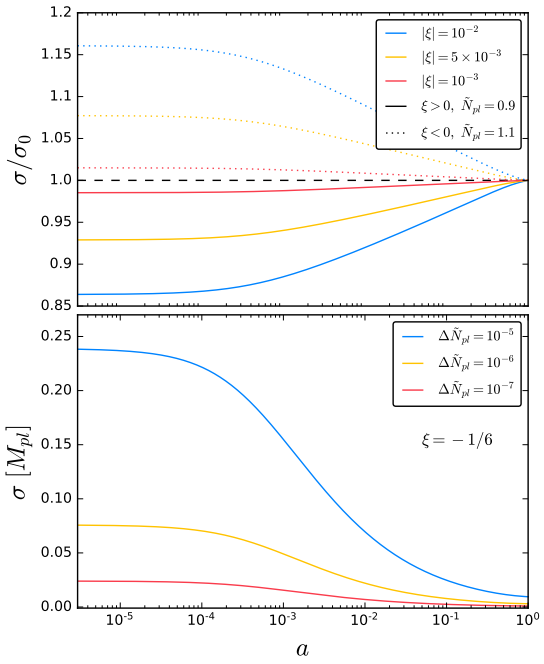

FIG. 1. Top panel: relative evolution of σ for different values of ξ. Bottom panel: evolution of σ for different values of N_{pl} for the CC case, i.e. $\xi = -1/6$.

$$
\begin{aligned}
\rho_{\rm DE} &= \frac{F_0}{F}\rho_\sigma + (\rho_m + \rho_r)\left(\frac{F_0}{F} - 1\right), && (15)\\
p_{\rm DE} &= \frac{F_0}{F}p_\sigma + p_r\left(\frac{F_0}{F} - 1\right). && (16)
\end{aligned}
$$

The effective parameter of state for DE can be defined as $w_{\rm DE} \equiv p_{\rm DE}/\rho_{\rm DE}$.

In Fig. 2 the evolution of this effective parameter of state is shown for different values of the parameters N_{pl} and ξ. In all the cases the parameter of state $w_{\rm DE}$ mimics $1/3$ (-1) in the relativistic era (at late times): this behaviour can be easily understood from Eq. (15) when ρ_r $(V(\sigma))$ dominates over the energy densities of other components. The behavious of $w_{\rm DE}$ at the onset of the matter dominated era is instead model dependent: for $\xi \neq -1/6$, we see that $w_{\rm DE} > 0$ from the upper two panels in Fig. 2, whereas for $\xi = -1/6$ we obtain $w_{\rm DE} \sim 1/3$ when $\sigma_0 \ll \sigma$. The absence of an intermediate phase of a matter dominated era for $\xi = -1/6$ is also clear in the initial conditions for the scale factor reported in Appendix A. It can be seen from Fig. 2 that there is no phantom behaviour of the effective DE component at small redshifts in contrast to more general scalar-tensor DE models studied in [32]. Indeed a phantom behaviour with $w_{\rm DE} < -1$ [32] is barely visible in the transient regime from the tracking value to $w_{\rm DE} \approx -1$ because of the small coupling ξ considered in Fig. 2 and cannot occur in the stable accelerating regime for these models with $V(\sigma) \propto F^2(\sigma)$.

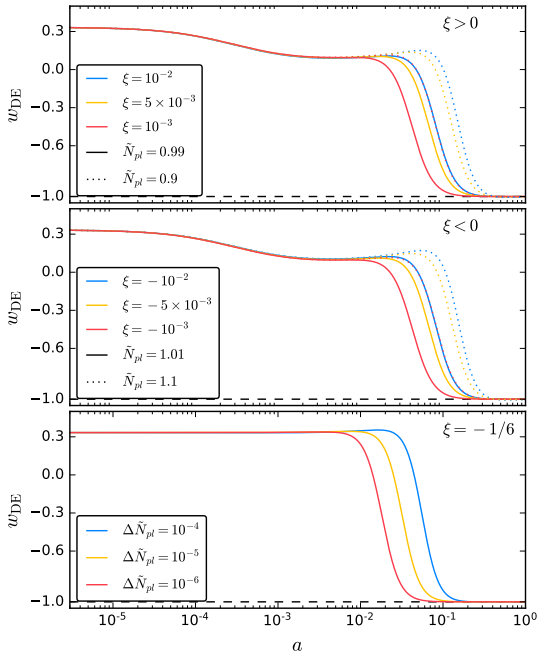

FIG. 2. Evolution of $w_{\rm DE}$ for different values of N_{pl} and ξ. We plot the effective parameter of state for DE for $\xi > 0$ in the upper panel, $\xi < 0$ in the central panel, and the CC case $\xi = -1/6$ in the bottom panel.

In Figs. 3-4-5, we show the evolution of the density parameters Ω_i, corresponding to an Einstein gravity system with a Newton's constant given by the current value of the scalar field today $G_N = 1/(8\pi F_0)$ [31] (also used in [3, 29]) for $\xi > 0$, $\xi < 0$ and $\xi = -1/6$, respectively.

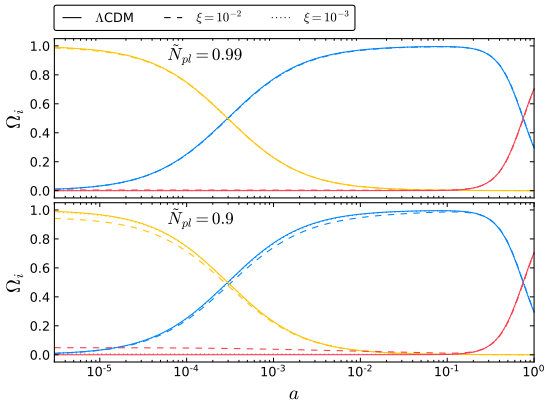

FIG. 3. Evolution of the density parameters Ω_i: radiation in yellow, matter in blue, and effective DE in red. We plot $\tilde{N}_{pl} = 1$ ($\tilde{N}_{pl} = 0.9$) for $\xi = 10^{-2}$, 10^{-3} in the top (bottom) panel.

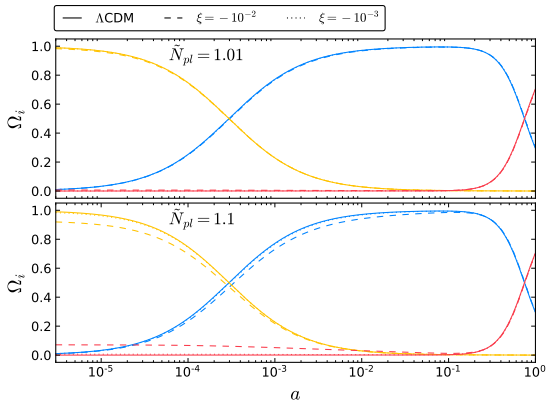

FIG. 4. Evolution of the density parameters Ω_i: radiation in yellow, matter in blue, and effective DE in red. We plot $\tilde{N}_{pl} = 1.01$ ($\tilde{N}_{pl} = 1.1$) for $\xi = -10^{-2}$, -10^{-3} in the top (bottom) panel.

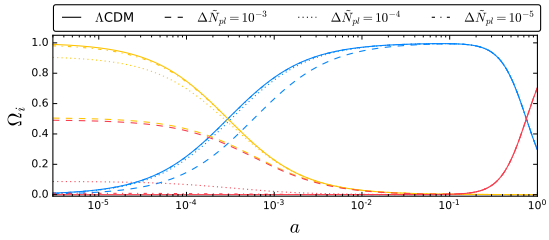

FIG. 5. Evolution of the density parameters Ω_i: radiation in yellow, matter in blue, and effective DE in red. We plot the CC case $\xi = -1/6$ for $\Delta\tilde{N}_{pl} = 10^{-3}$, 10^{-4}, 10^{-5}.

B. Boundary conditions for the the scalar field

As boundary conditions we impose that the effective Newton's constant at present is compatible with the Cavendish-like experiments. The effective gravitational constant for NMC is given by [31]:

$$G_{\rm eff} = \frac{1}{8\pi F}\left(\frac{2F + 4F_{,\sigma}^2}{2F + 3F_{,\sigma}^2}\right). \tag{17}$$

In Fig. 6 is shown the evolution of the relative effective gravitational constant (17). We can see that the effective gravitational constant decreases in time for all the choices of both N_{pl} and ξ.

We can distinguish three different cases beyond GR:

- $\tilde{N}_{pl} \to 0$ which is the IG case. This leads to:

$$\tilde{\sigma}_0^2 = \frac{1}{\xi}\frac{1+8\xi}{1+6\xi}, \tag{18}$$

  which is the same result as obtained in [3];

- $\xi \to -1/6$ which is the CC. In this particular case the polynomial equation (17) in σ_0 in quadratic and

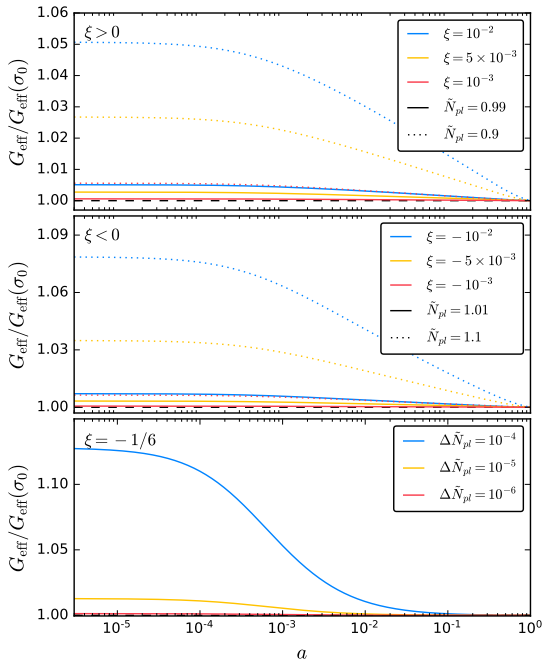

FIG. 6. Evolution of the effective gravitational constant $G_{\rm eff}$ relative to its value today for different values of N_{pl} and ξ. From top to bottom, the cases with $\xi > 0$, $\xi < 0$, and $\xi = -1/6$ are displayed, respectively.

we have:

$$\tilde{\sigma}_0^2 = \frac{18\tilde{N}_{pl}^2(\tilde{N}_{pl}^2-1)}{1+3\tilde{N}_{pl}^2}; \tag{19}$$

- a general NMC case for $\xi \neq -1/6$:

$$\tilde{\sigma}_0^2 = \frac{1-2\tilde{N}_{pl}^2+2\xi(4-3\tilde{N}_{pl}^2)}{2\xi(1+6\xi)} \pm \frac{\sqrt{1-4\xi(5\tilde{N}_{pl}^2-4)+4\xi^2(3\tilde{N}_{pl}^2-4)^2}}{2\xi(1+6\xi)}. \tag{20}$$

By requiring $\tilde{\sigma}^2 \geq 0$ and $F \geq 0$, we obtain conditions on the two parameters $\tilde{N}_{pl}$ and ξ for the physical solution:

$$\tilde{N}_{pl} < 1 \text{ for } \xi > 0\,, \tag{21}$$
$$\tilde{N}_{pl} > 1 \text{ for } \xi < 0\,. \tag{22}$$

C. Comparison with general relativity

The deviations from GR for a theory of gravitation are described by the so called post-Newtonian parameters. For NMC only the parameters $\gamma_{\rm PN}$ and $\beta_{\rm PN}$ differ from GR predictions, for which they both equal unity. In terms of these parameters the line element can be expressed as:

$$ds^2 = -(1+2\Phi-2\beta_{\rm PN}\Phi^2)dt^2+(1-2\gamma_{\rm PN}\Phi)dx_i dx^i. \tag{23}$$

These parameters are given within NMC by the following equations [31]:

$$\gamma_{\rm PN} = 1 - \frac{F_{,\sigma}^2}{F+2F_{,\sigma}^2}, \tag{24}$$
$$\beta_{\rm PN} = 1 + \frac{FF_{,\sigma}}{8F+12F_{,\sigma}^2}\frac{d\gamma_{\rm PN}}{d\sigma}. \tag{25}$$

We have $\gamma_{\rm PN} \leq 1$ and $\beta_{\rm PN} \leq 1$ for $\xi > 0$, whereas $\gamma_{\rm PN} \leq 1$ and $\beta_{\rm PN} \geq 1$ for $\xi < 0$.

In Figs. 7, 8 and 9, we show the evolution of these parameters for different values of N_{pl} and ξ. It is interesting to note how in the CC case $\gamma_{\rm PN}$ and $\beta_{\rm PN}$ approach the GR value more rapidly than for $\xi \neq -1/6$.

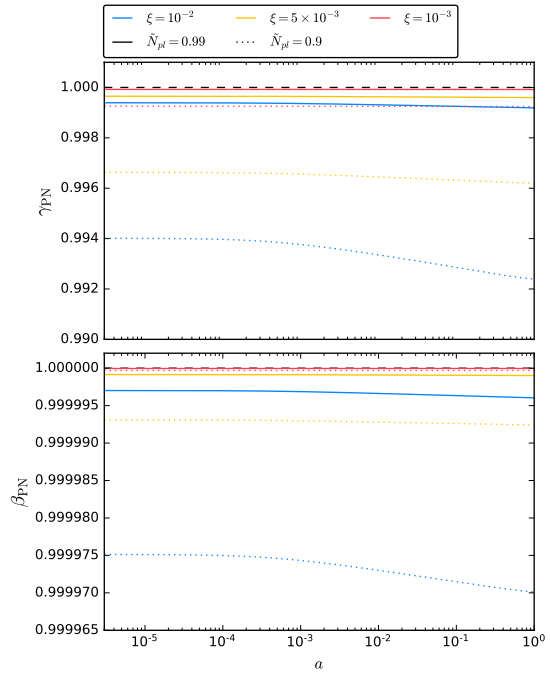

FIG. 7. Evolution of the post-Newtonian parameters $\gamma_{\rm PN}$ and $\beta_{\rm PN}$ for different values of N_{pl} and ξ. We show the case with $\xi > 0$.

III. LINEAR PERTURBATIONS

We study linear fluctuations around the FRW metric in the synchronous gauge:

$$ds^2 = a(\tau)^2\left[-d\tau^2 + (\delta_{ij}+h_{ij})dx^i dx^j\right], \tag{26}$$

where τ is the conformal time and h_{ij} include both the scalar (h_{ij}^S) and the tensor (h_{ij}^T) part. We follow the

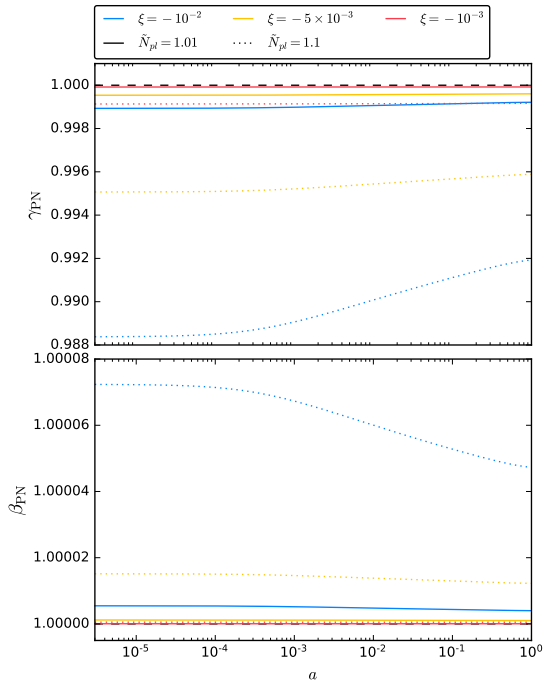

FIG. 8. Evolution of the post-Newtonian parameters $\gamma_{\rm PN}$ and $\beta_{\rm PN}$ for different values of N_{pl} and ξ. We show the NMC case with $\xi > 0$.

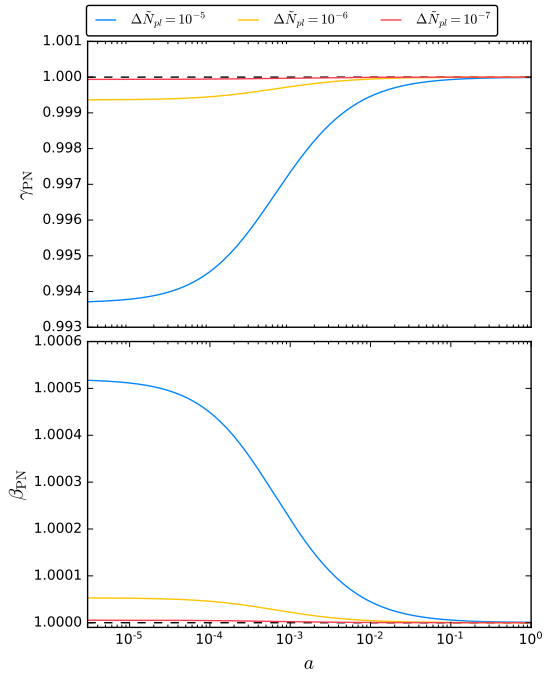

FIG. 9. Evolution of the post-Newtonian parameters $\gamma_{\rm PN}$ and $\beta_{\rm PN}$ for different values of N_{pl}. We show the NMC case $\xi = -1/6$, i.e. the CC case.

conventions of Ref. [33] for scalar metric perturbations h_{ij} and scalar field perturbation $\delta\sigma$:

$$h_{ij}^S = \int \mathrm{d}^3k\, e^{i\vec{k}\cdot\vec{x}} \Big[\hat{k}_i\hat{k}_j\, h(\vec{k},\tau) + \left(\hat{k}_i\hat{k}_j - \frac{1}{3}\delta_{ij}\right)\eta(\vec{k},\tau)\Big], \quad (27)$$

$$\delta\sigma = \int \mathrm{d}^3k\, e^{i\vec{k}\cdot\vec{x}}\delta\sigma(\vec{k},\tau). \quad (28)$$

In Fig. 10, we show the evolution of the scalar field perturbation $\delta\sigma$ at $k = 0.05$ Mpc^{-1} for different values of N_{pl} and ξ.

The modified Einstein equations in Eq. (3) at first order for scalar perturbations are:

$$\frac{k^2}{a^2}\eta - \frac{1}{2}H\dot{h} = -\frac{1}{2F}\left[\delta\rho + \dot{\sigma}\delta\dot{\sigma} + V_{,\sigma}\delta\sigma - \frac{F_{,\sigma}}{F}\left(\rho + \frac{\dot{\sigma}^2}{2} + V - 3H\dot{F}\right)\delta\sigma\right], \tag{29}$$

$$\frac{k^2}{a^2}\dot{\eta} = \frac{1}{2F}\left[\sum_i(\rho_i + p_i)\theta_i + k^2\left(\dot{\sigma}\delta\sigma + \delta\dot{F} - H\delta F\right)\right], \tag{30}$$

$$\ddot{h} + 3H\dot{h} - 2\frac{k^2}{a^2}\eta = -\frac{3}{F}\left[p + \dot{\sigma}\delta\dot{\sigma} - V_{,\sigma}\delta\sigma - \frac{F_{,\sigma}}{F}\left(p + \frac{\dot{\sigma}^2}{2} - V + \ddot{F} + 2H\dot{F}\right)\delta\sigma + \frac{2}{3}\frac{k^2}{a^2}\delta F + \delta\ddot{F} + 2H\delta\dot{F} + \frac{1}{3}\dot{h}\dot{F}\right], \tag{31}$$

$$\ddot{h} + 6\ddot{\eta} + 3H(\dot{h} + 6\dot{\eta}) - 2\frac{k^2}{a^2}\eta = -\frac{3}{F}\left[\sum_i(\rho_i + p_i)\sigma_i + \frac{2}{3}\frac{k^2}{a^2}\delta F + \frac{\dot{F}}{3}(\dot{h} + 6\dot{\eta})\right], \tag{32}$$

where all perturbations are considered in the Fourier configuration. The quantities θ_i and σ_i represent the velocity potential and the anisotropic stress, respectively. It can be seen from the last of these equations that the coupling function acts also as a source for the anisotropic stress.

The perturbed Klein-Gordon equation is:

$$\begin{aligned}\delta\ddot{\sigma} = &-\delta\dot{\sigma}\left[3H + \frac{2(1+6\xi)\xi\sigma\dot{\sigma}}{F + 6\xi^2\sigma^2}\right] - \delta\sigma\left\{\frac{k^2}{a^2} + \frac{FV_{,\sigma,\sigma}}{F + 6\xi^2\sigma^2} - \frac{2\xi\sigma V_{,\sigma}}{F + 6\xi^2\sigma^2}\left[1 + \frac{F(1+6\xi)}{F + 6\xi^2\sigma^2}\right]\right.\\ &\left. + \frac{\xi}{F + 6\xi^2\sigma^2}\left[1 - \frac{2(1+6\xi)\xi\sigma^2}{F + 6\xi^2\sigma^2}\right]\left[(1+6\xi)\dot{\sigma}^2 - 4V + (3p - \rho)\right]\right\} - \frac{(3\delta p - \delta\rho)\,\xi\sigma}{F + 6\xi^2\sigma^2} - \frac{1}{2}\dot{h}\dot{\sigma}.\end{aligned} \tag{33}$$

As for the homogeneous KG Eq. (12), the choice $V \propto F^2$ also leads to an effectively massless scalar field fluctuation. Both initial conditions for the background and for the linear perturbations at the next-to-leading order in τ are shown in the Appendix A. We consider adiabatic initial condition for the scalar cosmological fluctuations [3, 34].

Analogously, the transverse and traceless part of the metric fluctuation h_{ij}^T is expanded as:

$$h_{ij}^T = \int \mathrm{d}^3k e^{i\vec{k}\cdot\vec{x}}\left[h_+ e_{ij}^+ + h_\times e_{ij}^\times\right], \tag{34}$$

where h_+, h_- and $e^+, e^\times$ are the amplitude and normalized tensors of the two independent states to the direction of propagation of gravitational waves in Fourier space. The evolution equation for the amplitude is:

$$\ddot{h}_{s,k} + \left(3H + \frac{\dot{F}}{F}\right)\dot{h}_{s,k} + \frac{k^2}{a^2}h_{s,k} = \frac{2}{F}\rho_\nu\pi^\nu \tag{35}$$

where s denote the two polarization state of the two independent modes ($s = +, \times$) and the right hand side denotes the contribution of the traceless and transverse part of the neutrino anisotropic stress. The importance of the extra-damping term in the evolution equation for gravitational waves has been previously stressed [35, 36]. The example of the impact of this term with respect to GR is depicted in Fig. 11. Note that the parameters cho-

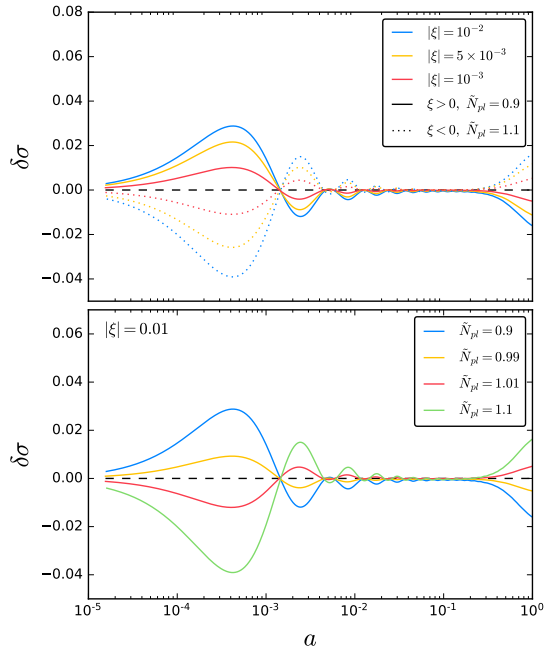

FIG. 10. Evolution of scalar field perturbations in the synchronous gauge for $k = 0.05$ Mpc^{-1}.

sen are compatible with the previous figures in this paper and we are therefore in a regime in which $\dot{F}/F \ll 3H$.

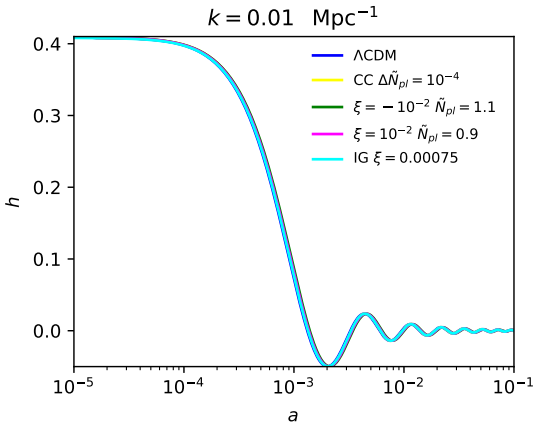

FIG. 11. Evolution of tensor fluctuations h^T for $k = 0.01$ Mpc^{-1}.

IV. CMB ANISOTROPIES AND MATTER POWER SPECTRA

The footprints of these scalar-tensor theories into the CMB anisotropies angular power spectra can be understood as a generalization of the effects in eJBD or equivalently IG theories. The redshift of matter-radiation equality is modified in scalar-tensor theories by the motion of the scalar field driven by pressureless matter and this results in a shift of the CMB acoustic peaks for values $\xi \neq 0$, as for the IG case [7, 37]. In addition, a departure from $\tilde{N}_{pl} = 1$ induces a further change both in the amplitude of the peaks and their positions. We note that decreasing the value of $\tilde{N}_{pl}$ is possible to suppress the deviations with respect to the ΛCDM model allowing for larger values of the coupling ξ compared to the IG case.

We show the relative differences with respect to the ΛCDM model for the lensed CMB angular power spectra anisotropies in temperature and E-mode polarization, and the CMB lensing angular power spectra for different values of N_{pl} for $\xi > 0$ in Fig. 12, $\xi < 0$ in Fig. 13, and the CC case $\xi = -1/6$ in Fig. 14. We show also the absolute difference of the TE cross-correlation weighted by the square root of the product of the two auto-correlators.

In Fig. 15 we show the relative differences for the matter power spectrum at $z = 0$ with respect to the ΛCDM model for different values of the parameters. In all the cases the $P(k)$ is enhanced at small scales, i.e. $k \gtrsim 0.01$ h Mpc^{-1}, compared to the ΛCDM model.

We end this section by discussing the B-mode polarization power spectra resulting from the evolution of tensor fluctuations in Eq. 35. Fig. 16 shows the comparison of the tensor and lensing contributions to B-mode polarization in ΛCDM GR and the scalar-tensor cases of IG

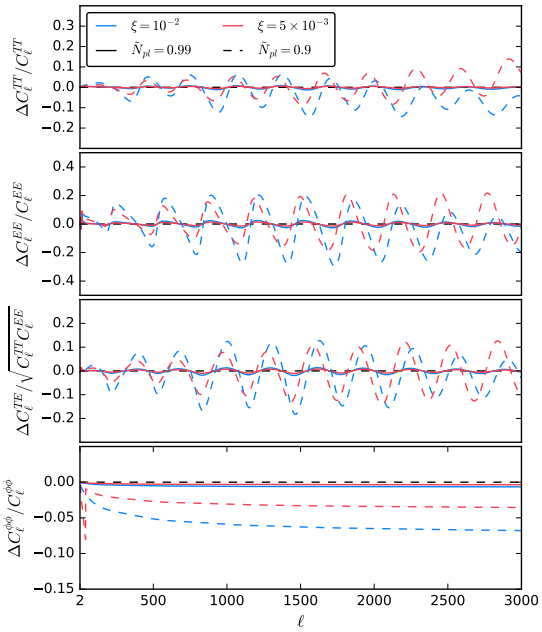

FIG. 12. From top to bottom: relative differences of the TT-EE-TE-$\phi\phi$ power spectra with respect to the ΛCDM model for $\tilde{N}_{pl} = 1$, 0.9 and different values of $\xi = 10^{-2}$, 5×10^{-3}.

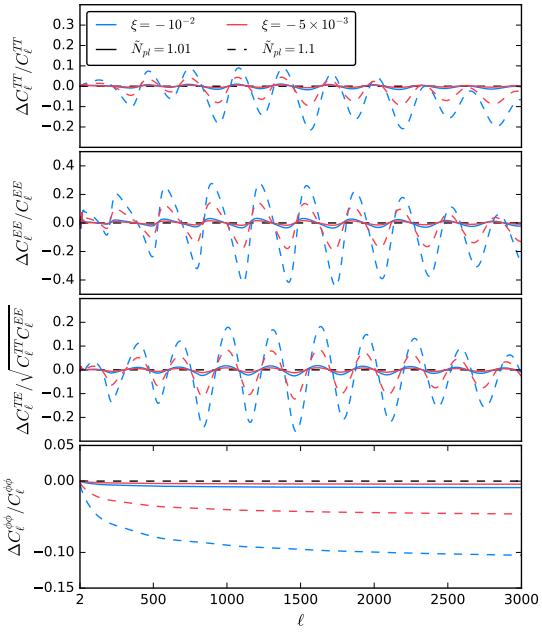

FIG. 13. From top to bottom: relative differences of the TT-EE-TE-$\phi\phi$ power spectra with respect to the ΛCDM model for $\tilde{N}_{pl} = 1.01$, 1.1 and different values of $\xi = -10^{-2}$, -5×10^{-3}.

($N_{\rm pl} = 0$), CC ($\xi = -1/6$), positive and negative ξ for a value of a tensor-to-scalar ratio $r = 0.05$, compatible with the most recent constraints [38, 39]. It is important to note that for the values of the couplings chosen

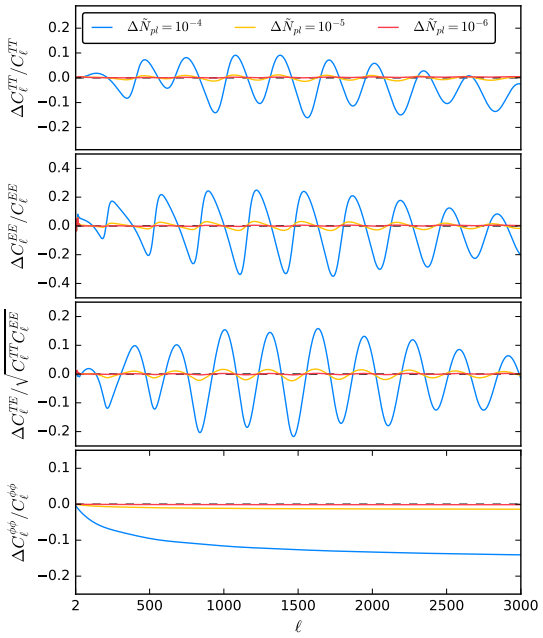

FIG. 14. From top to bottom: relative differences of the TT-EE-TE-$\phi\phi$ power spectra with respect to the ΛCDM model for the CC case, i.e. $\xi = -1/6$, with different values of $\Delta\tilde{N}_{pl} = 10^{-4}$, 10^{-5}, 10^{-6}.

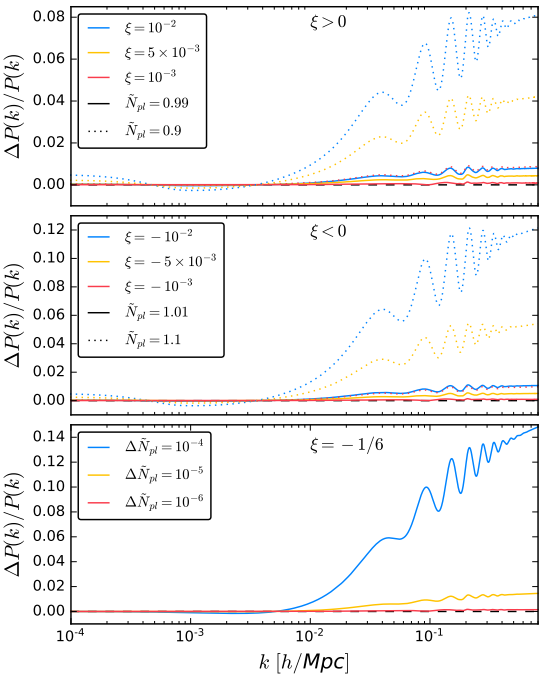

FIG. 15. From top to bottom: relative differences of the matter power spectra at $z = 0$ with respect to the ΛCDM model for $\xi > 0$, $\xi < 0$ and $\xi = -1/6$.

in Fig. 16 the main differences in the tensor contribution to B-mode polarization with respect to ΛCDM GR case is due to the different evolution in the Hubble parameter and in the transfer functions in the definition of CMB anisotropies.

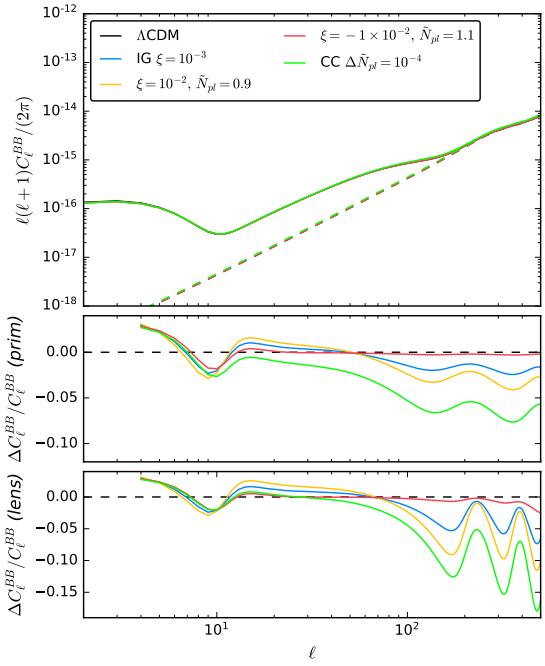

FIG. 16. From top to bottom: CMB B-mode polarization band power, relative differences of the tensor contribution, and relative differences of the lensing contribution with respect to the ΛCDM model for $\xi > 0$, $\xi < 0$, $\xi = -1/6$, and IG. Dashed lines refer to the lensing contribution to the B-mode polarization angular power spectrum.

V. CONSTRAINTS FROM COSMOLOGICAL OBSERVATIONS

We perform a Monte Carlo Markov Chain analysis by using the publicly available code `MontePython` † [40, 41] connected to our modified version of the code `CLASS` ‡ [42], i.e. `CLASSig` [3].

We use *Planck* 2015 and BAO likelihoods. We combine the *Planck* high-ℓ ($\ell > 29$) temperature data with the joint temperature-polarization low-ℓ ($2 \leq \ell \leq 29$) likelihood in pixel space at a resolution of 3.7 deg, i.e. `HEALPIX` Nside=16 [43]. The *Planck* CMB lensing likelihood in the conservative multipoles range, i.e. $40 \leq \ell \leq 400$ [44] from the publicly available *Planck* 2015 release is also combined. We use BAO data to complement CMB anisotropies at low redshift: we include measurements of D_V/r_s at $z_{\rm eff} = 0.106$ from 6dFGRS [45], at $z_{\rm eff} = 0.15$

† https://github.com/brinckmann/montepython_public
‡ https://github.com/lesgourg/class_public

from SDSS-MGS [46], and from SDSS-DR11 CMASS and LOWZ at $z_{\rm eff} = 0.57$ and $z_{\rm eff} = 0.32$, respectively [47].

We sample with linear priors the six standard cosmological parameters, i.e. $\omega_{\rm b} \equiv \Omega_{\rm b}h^2$, $\omega_{\rm c} \equiv \Omega_{\rm c}h^2$, H_0, $\tau_{\rm re}$, $\ln\left(10^{10}A_{\rm s}\right)$, and $n_{\rm s}$, plus the two extra parameters for a non-minimally coupled scalar field, i.e. $\Delta\tilde{N}_{\rm pl}$ and ξ. In the analysis we assume massless neutrinos and marginalize over *Planck* high-ℓ likelihood foreground and calibration nuisance parameters [43] which are allowed to vary.

As in [4], we take into account the change of the cosmological abundances of the light elements during Big Bang Nucleosynthesis (BBN) induced by a different gravitational constant during the radiation era with respect the theoretical prediction obtained from the public code `PArthENoPE` [48]. We take into account the modified BBN consistency condition due to the different value of the effective gravitational constant during BBN, by considering this effect as modelled by dark radiation, since the latter effect is already tabulated as $Y_{\rm P}^{\rm BBN}(\omega_b, N_{\rm eff})$ [49] in the public version of the `CLASS` code. As in [4], the posterior probabilities for the primary cosmological parameters are hardly affected by the modified BBN consistency condition, and we report a small shift for the primordial Helium abundance to higher values.

A. Results

The results from our MCMC exploration are summarized in Table I. We find for the positive branch of the coupling at 95% CL:

$$N_{pl} > 0.81\ [\mathrm{M}_{pl}], \tag{36}$$
$$\xi < 0.064. \tag{37}$$

We show in Fig. 17 a zoom of the 2D parameter space (H_0, ξ) comparing the result of NMC to IG, i.e. $N_{pl} = 0$. The constraint on ξ is degradated by almost two order of magnitude ($\xi < 0.0075$ at 95% CL for IG [4]) due to the strong degeneracy between N_{pl} and ξ, see Fig. 18.

The constraints for the negative branch are (see Figs. 19-20):

$$N_{pl} < 1.39\ [\mathrm{M}_{pl}], \tag{38}$$
$$\xi > -0.11. \tag{39}$$

at the 95% CL for *Planck* TT + lowP + lensing + BAO.

We quote also the derived constraints on the change of the effective Newton's constant (17) evaluated between the radiation era and the present time, and also its derivative at present time at 95% CL:

$$\frac{\delta G_{\rm eff}}{G} > -0.027\,, \tag{40}$$
$$\frac{\dot{G}_{\rm eff}}{G}(z=0) > -1.4\left[\times 10^{-13}\,\mathrm{yr}^{-1}\right]\,, \tag{41}$$

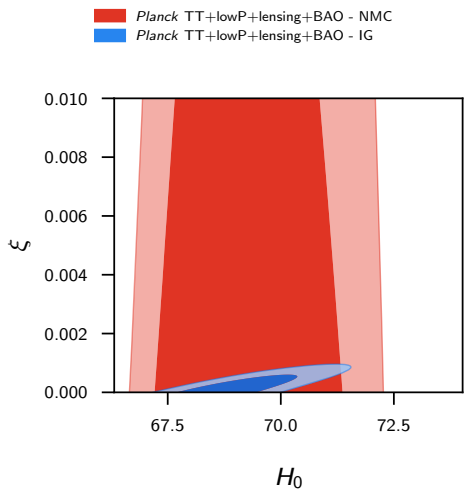

FIG. 17. 2D marginalized confidence levels at 68% and 95% for (H_0, ξ) for NMC $\xi > 0$ (red) and IG (blue) with *Planck* TT + lowP + lensing + BAO.

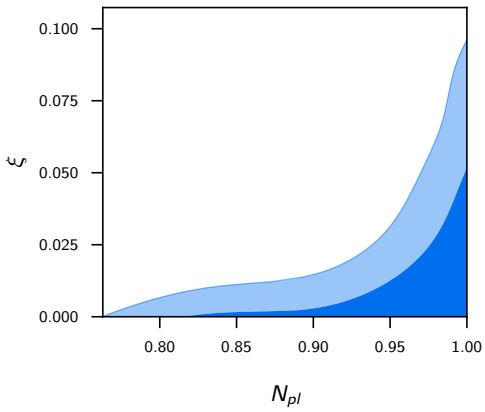

FIG. 18. 2D marginalized confidence levels at 68% and 95% for (N_{pl}, ξ) for NMC $\xi > 0$ with *Planck* TT + lowP + lensing + BAO.

for $\xi > 0$, and:

$$\frac{\delta G_{\rm eff}}{G} > -0.027\,, \tag{42}$$
$$\frac{\dot{G}_{\rm eff}}{G}(z=0) > -0.97\left[\times 10^{-13}\,\mathrm{yr}^{-1}\right]\,, \tag{43}$$

for $\xi < 0$.

For the CC case, i.e. fixing $\xi = -1/6$, results are listed in Tab. II. This model is severely constrained by data leading to tight upper bound on N_{pl} at 95% CL:

$$1 < N_{pl} < 1.000038\ [\mathrm{M}_{pl}], \tag{44}$$

where $\tilde{N}_{pl}$ can take only values larger than one in this case.

	Planck TT + lowP + lensing + BAO ΛCDM	*Planck* TT + lowP + lensing + BAO IG	*Planck* TT + lowP + lensing + BAO ($\xi > 0$)	*Planck* TT + lowP + lensing + BAO ($\xi < 0$)
$\omega_{\rm b}$	0.02225 ± 0.00020	$0.02224^{+0.00020}_{-0.00021}$	0.02226 ± 0.00019	0.02226 ± 0.00021
$\omega_{\rm c}$	0.1186 ± 0.0012	0.1191 ± -0.0014	0.1190 ± 0.0015	0.1189 ± 0.0015
H_0 [km s^{-1} Mpc^{-1}]	67.78 ± 0.57	$69.4^{+0.7}_{-0.9}$	$69.2^{+0.8}_{-1.1}$	$69.2^{+0.7}_{-1.0}$
$\tau_{\rm re}$	0.066 ± 0.012	$0.063^{+0.012}_{-0.014}$	0.068 ± 0.014	0.069 ± 0.013
$\ln(10^{10} A_{\rm s})$	3.062 ± 0.024	$3.059^{+0.022}_{-0.026}$	$3.069^{+0.023}_{-0.027}$	3.071 ± 0.024
$n_{\rm s}$	0.9675 ± 0.0045	$0.9669^{+0.0042}_{-0.0047}$	0.9674 ± 0.0046	0.9728 ± 0.0043
ξ	...	< 0.00075 (95% CL)	< 0.064 (95% CL)	> -0.011 (95% CL)
N_{pl} [M$_{pl}$]	...	0	> 0.81 (95% CL)	< 1.39 (95% CL)
$\gamma_{\rm PN}$	1	> 0.9970 (95% CL)	> 0.995 (95% CL)	> 0.997 (95% CL)
$\beta_{\rm PN}$	1	1	> 0.99987 (95% CL)	< 1.000011 (95% CL)
$\delta G_{\rm N}/G_{\rm N}$	...	$-0.009^{+0.003}_{-0.009}$	> -0.027 (95% CL)	> -0.027 (95% CL)
$10^{13}\,\dot{G}_{\rm N}(z=0)/G_{\rm N}$ [yr^{-1}]	...	-0.37^{+34}_{-12}	> -1.4 (95% CL)	> -0.97 (95% CL)

TABLE I. Constraints on main and derived parameters for *Planck* TT + lowP + lensing + BAO (at 68% CL if not otherwise stated). In the first column we report the results obtained for the branch with $\xi > 0$ and in the second the branch for $\xi < 0$. In the first column we report the results obtained for the ΛCDM model with the same dataset [50] and in the second column IG case, i.e. $N_{pl} = 0$, for comparison [4].

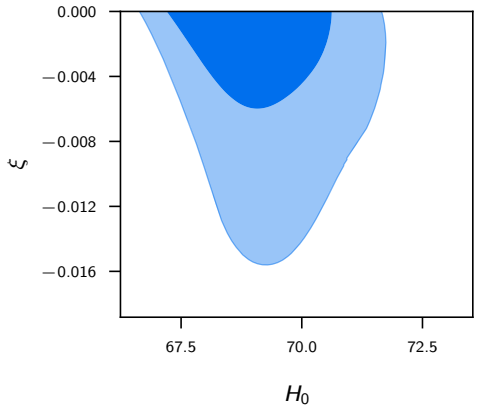

FIG. 19. 2D marginalized confidence levels at 68% and 95% for (H_0, ξ) for NMC $\xi < 0$ with *Planck* TT + lowP + lensing + BAO.

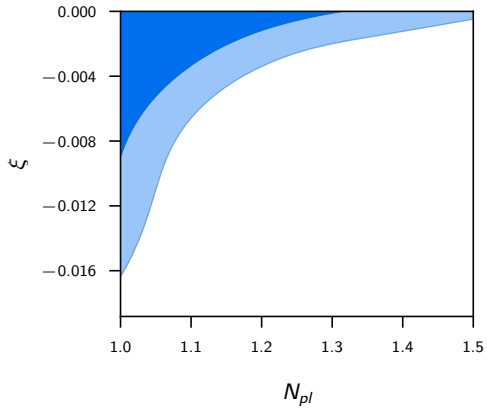

FIG. 20. 2D marginalized confidence levels at 68% and 95% for (N_{pl}, ξ) for NMC $\xi < 0$ with *Planck* TT + lowP + lensing + BAO.

All these models provide a fit to *Planck* 2015 and BAO data very similar to ΛCDM: we report $\Delta\chi^2 \sim -2.6$ for all the models considered in this paper. Due to the limited improvement in $\Delta\chi^2$, none of these models is preferred at a statistically significant level with respect to ΛCDM.

B. The Hubble parameter

We find constraints compatible with the ΛCDM values for the standard cosmological parameters. However, the shifts in H_0 deserve a particular mention: as already remarked in [3, 4] for the IG case, the mean values for H_0 are larger for all the models studied here. Fig. 21 shows how the 2D marginalized contours for (H_0, N_{pl}) have a degeneracy. We find:

$$H_0 = 69.19^{+0.77}_{-0.93}\ [\rm km/s/Mpc], \tag{45}$$

This value is larger, but compatible at 2σ level with the ΛCDM value ($H_0 = 67.78 \pm 0.57$ [km/s/Mpc]). However, it is still lower than the local measurement of the Hubble constant [51] ($H_0 = 73.52 \pm 1.62$ [km/s/Mpc]) obtained by including the new MW parallaxes from HST and Gaia to the rest of the data from [52]. Therefore the tension between the model dependent estimate of the Hubble parameter from *Planck* 2015 plus BAO data and the local measurement from [51] decreases to 2.3σ from the 3.3σ of the ΛCDM model. For comparison, by varying the number degree of relativistic species $N_{\rm eff}$ in Einstein gravity, a lower value for the Hubble parameter, i.e. $H_0 = 68.00 \pm 1.5$ [km/s/Mpc] (with $N_{\rm eff} = 3.08^{+0.22}_{-0.24}$) for *Planck* TT + lowP + lensing + BAO at 68% CL, is

	Planck TT + lowP + lensing + BAO	*Planck* TT + lowP + lensing + BAO + HST
$\omega_{\rm b}$	0.02223 ± 0.00021	0.02228 ± 0.00021
$\omega_{\rm c}$	$0.1188^{+0.0014}_{-0.0015}$	0.1187 ± 0.0015
H_0 [km s^{-1} Mpc^{-1}]	$69.19^{+0.77}_{-0.93}$	70.20 ± 0.83
$\tau_{\rm re}$	$0.068^{+0.012}_{-0.014}$	$0.070^{+0.013}_{-0.015}$
$\ln(10^{10} A_{\rm s})$	3.070 ± 0.024	3.074 ± 0.024
$n_{\rm s}$	0.9699 ± 0.0045	0.9728 ± 0.0043
N_{pl} [M_{pl}]	< 1.000038 (95% CL)	$1.000028^{+0.000012}_{-0.000014}$
$\gamma_{\rm PN}$	> 0.99996 (95% CL)	1.00003 ± 0.00001
$\beta_{\rm PN}$	< 1.000003 (95% CL)	0.999998 ± 0.000001

TABLE II. Constraints on main and derived parameters for *Planck* TT + lowP + lensing + BAO in the case of the CC model (at 68% CL if not otherwise stated).

obtained compared to the CC case reported in Eq. (45). When the local measurement of the Hubble constant [51] is included in the fit we obtain:

$$H_0 = 70.20 \pm 0.83 \ [\mathrm{km/s/Mpc}], \tag{46}$$

$$N_{pl} = 1.000028^{+0.000012}_{-0.000014} \ [\mathrm{M}_{pl}] \, . \tag{47}$$

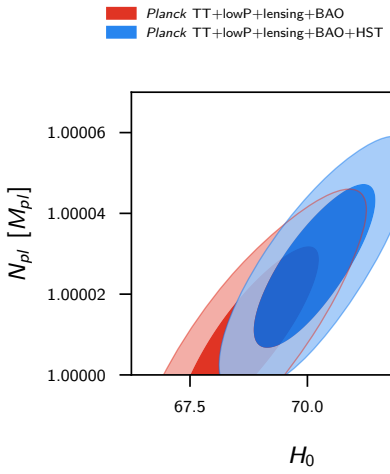

FIG. 21. 2D marginalized confidence levels at 68% and 95% for (H_0, N_{pl}) for conformal coupling with *Planck* TT + lowP + lensing + BAO. We include in blue the local estimates of $H_0 = 73.52 \pm 1.62$ [km/s/Mpc] [51].

Since the marginalized value for H_0 in either eJBD and NMC models is larger than in common extensions of the ΛCDM model [50], such as ΛCDM + $N_{\rm eff}$, it is useful to understand how the evolution of the Hubble parameter differ at early and late times. The differences at early time can be easily understood: since the effective Newton's constant can only decrease, if we consider the same H_0, this will correspond to an higher $H(z)$ or to a larger $N_{\rm eff}$ in the radiation era compared to the ΛCDM. A second effect around recombination is the motion of the scalar field driven by pressureless matter. At lower

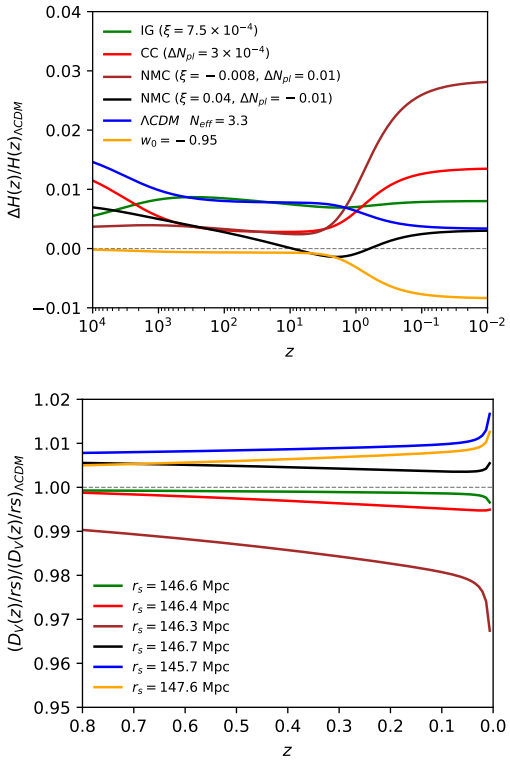

FIG. 22. Redshift evolution for relative difference between the Hubble parameter $H(z)$ and its ΛCDM counterpart (upper panel) and the ratio $D_V(z)/r_s$ (lower panel). For ΛCDM quantities we used *Planck* TT + lowP + lensing + BAO best-fit. The models plotted are IG, CC, $\xi < 0$, $\xi > 0$, ΛCDM model with $N_{\rm eff} > 3.046$ and wCDM with $w_0 = \mathrm{const} \neq 0$ for green, red, brown, black, blue and orange lines respectively.

redshifts, the differences with respect to ΛCDM are originated by the onset of the acceleration stage by σ. The upper panel of Fig. 22 shows relative differences of $H(z)$ with respect to the *Planck* TT + lowP + lensing + BAO ΛCDM best-fit: best-fit (for IG) or NMC models within the 1σ contours are compared with ΛCDM + $N_{\rm eff}$ or wCDM. This plot shows how in these scalar-tensor models both early and late time dynamics can contribute to a larger value for H_0 than in ΛCDM + $N_{\rm eff}$, for example.

However, because of this contribution from late time dynamics, the change in H_0 cannot be interpreted only as a proportional decrement in the comoving sound horizon at the baryon drag epoch r_s, which is the quantity used to calibrate the BAO standard ruler and is 147.6 Mpc for ΛCDM with the data considered. The bottom panel of Fig. 22 shows $D_V(z)/r_s \equiv \frac{[cz(1+z)^2 D_A(z)^2 H(z)^{-1}]^{1/3}}{r_s}$, with D_A as the angular diameter distance, normalized to its ΛCDM value, and the value of r_s. It is easy to see that both r_s and H_0 are lower for ΛCDM + $N_{\rm eff}$ than for the scalar-tensor models studied here and the eJBD model. These scalar-tensor models therefore differ from those which aim in reducing the tension between CMB anisotropies and the local measurements of H_0 through

a decrement of r_s [53–55], such as those in which ultra-light axion fields move slowly around recombination and then dilute away [56–58]. In the scalar-tensor models considered here the scalar field moves naturally around recombination since is forced by pressureless matter and dominates at late time acting as DE.

C. Constraints on the post-Newtonian parameters

Finally, we quote the derived constraints on the post-Newtonian parameters. In this class of models $\gamma_{\rm PN}$, $\beta_{\rm PN} \neq 1$ according to Eqs. (24)-(25) at 95% CL:

$$0.995 < \gamma_{\rm PN} < 1, \ (\xi > 0) \tag{48}$$
$$0.99987 < \beta_{\rm PN} < 1, \tag{49}$$

$$0.997 < \gamma_{\rm PN} < 1, \ (\xi < 0) \tag{50}$$
$$1 < \beta_{\rm PN} < 1.000011. \tag{51}$$

See Fig. 23 for the 2D marginalized constraints in the $(\gamma_{\rm PN}, \beta_{\rm PN})$ plane. See Fig. 24 for the 2D marginalized constraints in the $(H_0, \gamma_{\rm PN})$ plane for $\xi > 0$ compared to the IG case studied in [4].

The tight constraint on N_{pl} for the CC case correspond at 95% CL to:

$$0 < 1 - \gamma_{\rm PN} < 4 \times 10^{-5}, \tag{52}$$
$$0 < \beta_{\rm PN} - 1 < 3 \times 10^{-6}, \tag{53}$$

for *Planck* TT + lowP + lensing + BAO, where the latter is tighter than the constraint from the perihelion shift $\beta_{\rm PN} - 1 = (4.1 \pm 7.8) \times 10^{-5}$ [59] and the former is twice the uncertainty of the Shapiro time delay constraint $\gamma_{\rm PN} - 1 = (2.1 \pm 2.3) \times 10^{-5}$ [60].

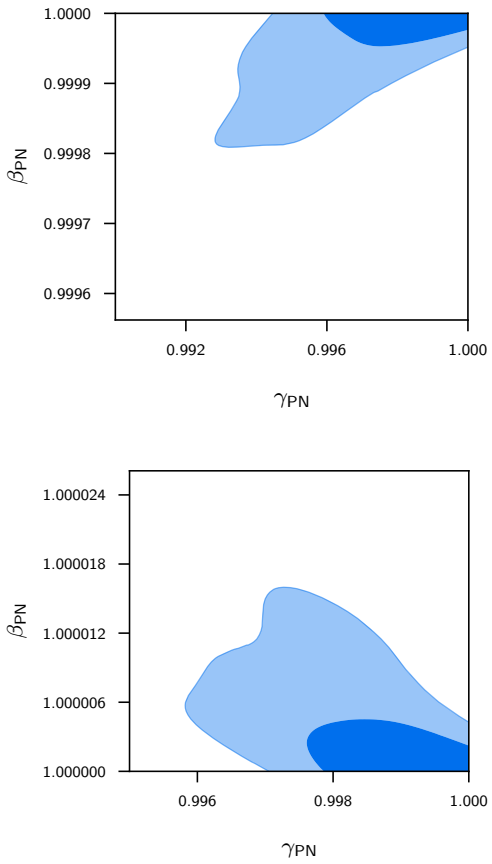

FIG. 23. 2D marginalized confidence levels at 68% and 95% for ($\gamma_{\rm PN}$, $\beta_{\rm PN}$) for NMC $\xi > 0$ (left panel) and $\xi < 0$ (right panel) with *Planck* TT + lowP + lensing + BAO

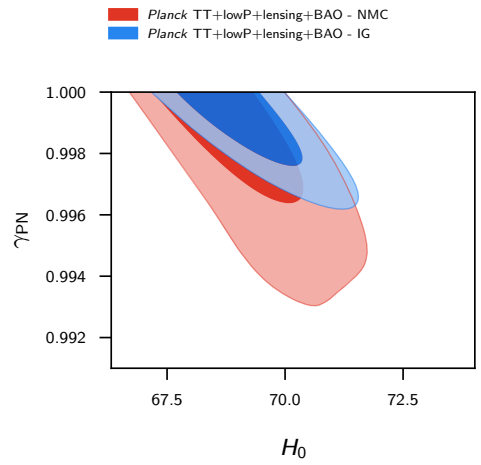

FIG. 24. 2D marginalized confidence levels at 68% and 95% for (H_0, $\gamma_{\rm PN}$) for NMC $\xi > 0$ (red) and IG (blue) with *Planck* TT + lowP + lensing + BAO.

VI. CONCLUSIONS

We have expanded on our previous study of the observational predictions within the eJBD theory or, equivalently, IG [3, 4], to the case of a scalar field nonminimally coupled to the Einstein gravity as in Eq. (1) with $G_3 = G_5 = 0$ and $2G_4 = F(\sigma) = N_{pl}^2 + \xi\sigma^2$. We have studied this class of model under the assumption that the effective gravitational constant in these scalar-tensor theories is compatible with the one measured in a Cavendish-like experiment. Whereas in the eJBD theory only the first post-Newtonian parameter $\gamma_{\rm PN}$ $(= 1 - \frac{F_{,\sigma}^2}{F + 2F_{,\sigma}^2})$ is not vanishing, in this simple extension both the first and second post-Newtonian parameter $\beta_{\rm PN}$ $(= 1 + \frac{F\,F_{,\sigma}}{8F + 12F_{,\sigma}^2}\frac{d\gamma_{\rm PN}}{d\sigma})$ are non-zero. The second post-Newtonian parameters encodes the sign of the coupling to gravity, i.e. $\beta_{\rm PN} > 0$ (< 0) for $\xi > 0$ $(\xi < 0)$.

For the sake of semplicity, we have restricted ourselves to the class of potential $V(\sigma) \propto F^2(\sigma)$, which makes the field effectively massless [19] and allows for a direct comparison with the IG model for $N_{pl} = 0$ [3, 4, 28, 29, 61].

For this choice of potential $V(\sigma) \propto F^2(\sigma)$, the scalar field is effectively massless. By assuming natural initial conditions in which the decaying mode is negligible, the scalar field starts at rest deep in the radiation era and is pushed by pressureless matter to the final stage in which it drives the Universe in a nearly de Sitter stage at late times with $\sigma = $ const. In general the effective parameter of state $w_{\rm DE}$ for σ defined in [31] tracks the one of the dominant matter component before reaching -1 once the Universe enters in the accelerated stage as for the IG case. We find that the conformal case $\xi = -1/6$ is an exception to this general trend: for such a value the effective parameter of state $w_{\rm DE}$ interpolates between $1/3$ and -1 without an intermediate pressureless stage. Irrespective of the sign of the coupling ξ, $G_N(a) = 1/(8\pi F)$ decrease with time for this class of potential.

As in our previous works in IG, we have considered adiabatic initial conditions for fluctuations [3, 4, 62] which are derived in this work for a non-minimally coupled scalar field. By extending the modification of `CLASSig` [3] to a generic coupling $F(\sigma)$, we have derived the CMB temperature and polarization anisotropies and the matter power spectrum. Since the effective Newton's constant decrease in time after the relativistic era, we observe a shift of the acoustic peaks to higher multipoles and an excess in the matter power spectrum at $k \gtrsim 0.01$ Mpc^{-1} proportional to the deviation from GR.

We have used *Planck* 2015 and BAO data to constrain this class of models. As for IG, we obtain a marginalized value for H_0 higher than in ΛCDM for all these models, potentially alleviating the tension with the local measurement of the Hubble parameter obtained by calibrating with the Cepheids [51]. The goodness of fit to *Planck* 2015 plus BAO data provided by the models studied in this paper is quantitative similar to ΛCDM: since they have one (for the conformal coupled case $\xi = -1/6$) or two (for ξ allowed to vary) extra parameters, these models are not preferred with respect to ΛCDM. We have derived 95% CL upper bounds $\xi < 0.064$ ($|\xi| < 0.11$) and $0.81 < N_{pl} < 1$ ($1 < N_{pl} < 1.39$) for $\xi > 0$ ($\xi < 0$). It is interesting to note that the bound on $\gamma_{\rm PN}$ and $\delta G_{\rm eff}/G$ have just a small degradation with respect to eJBD with the same data set ($0.997 < \gamma_{\rm PN} < 1$ [4]). Overall, some cosmological constraints do not seem strongly dependent on the assumption $\beta_{\rm PN} = 0$ and have a large margin of improvement with future observations [14]. Although model dependent, cosmological observations seem more promising than other independent ways to test scalar-tensor theories in the strong gravity regime as the search for the presence of scalar polarization states of gravitational waves [63], which is also strongly constrained by LIGO/Virgo [64].

The conformal value $\xi = -1/6$ is an interesting and particular case which stands out within the general class of non-minimally coupled scalar fields. In addition to what already remarked about its effective parameter of state, we find that *Planck* 2015 + BAO data constrain quite tightly the conformal case with $V(\sigma) \propto F^2(\sigma)$: as 95% CL intervals, we find $1 < 10^5 \Delta\tilde{N}_{\rm Pl} < 3.8$, or equivalently $0.99996 < \gamma_{\rm PN} < 1$, $1 < \beta_{\rm PN} < 1.000003$, in terms of the post-Newtonian parameters. These tight cosmological constraints for the conformal case are comparable to those of obtained within the Solar System bounds [60].

As from Figs. 12-13-14-16 CMB polarization anisotropies have a greater sensitivity to the variation of the gravitational strength in these models. It will be therefore interesting to see the impact of the latest and more robust measurement of CMB polarization anisotropies from Planck [65–67] and from BICEP2/Keck Array [65] as well as of the more recent BAO data on the constraints of these models.

ACKNOWLEDGMENTS

We would like to thank Lloyd Knox and Vivian Poulin for discussions. MBa was supported by the South African Radio Astronomy Observatory, which is a facility of the National Research Foundation, an agency of the Department of Science and Technology and he was also supported by the Claude Leon Foundation. MBa, MBr, FF and DP acknowledge financial contribution from the agreement ASI/INAF n. 2018-23-HH.0 "Attività scientifica per la missione EUCLID – Fase D". FF and DP acknowledge also financial support by ASI Grant 2016-24-H.0. AAS was partly supported by the program KP19-270 "Questions of the origin and evolution of the Universe" of the Presidium of the Russian Academy of Sciences. This research used computational resources of the National Energy Research Scientific Computing Center (NERSC) and of INAF OAS Bologna.

Appendix A: Initial Conditions

Here we report the initial conditions adopted in this paper for a non-minimally coupled scalar field, which generalize the case of adiabatic initial conditions for IG presented in [62]. These quantities reduces to IG and general relativity cases for $N_{pl} = 0$ and $(N_{pl} = M_{pl}, \xi = 0)$, respectively.

For the background cosmology we have as initial conditions:

$$a(\tau) = \sqrt{\frac{\rho_{r0}}{3F_i}}\tau \left[1 + \frac{\omega}{4}\tau - \frac{5}{16}\frac{\xi^2\sigma_i^2(1+6\xi)}{F_i + 6\xi^2\sigma_i^2}\omega^2\tau^2\right], \tag{A1}$$

$$\mathcal{H}(\tau) = \frac{1}{\tau}\left[1 + \frac{\omega}{4}\tau - \frac{1}{16}\frac{F_i + 4\xi^2\sigma_i^2(4+15\xi)}{F_i + 6\xi^2\sigma_i^2}\omega^2\tau^2\right], \tag{A2}$$

$$\sigma(\tau) = \sigma_i\left[1 + \frac{3}{2}\xi\omega\tau - \frac{2F_i(1-3\xi) + 27\xi^2\sigma_i^2(1+2\xi)}{8(F_i + 6\xi^2\sigma_i^2)}\omega^2\tau^2\right], \tag{A3}$$

where $\omega = \frac{\rho_{m0}}{\sqrt{3\rho_{r0}}}\frac{\sqrt{F_i}}{F_i+6\xi^2\sigma_i^2}$.

For cosmological fluctuations in the synchronous gauge we have as adiabatic initial conditions:

$$\delta_\gamma(k,\tau) = \delta_\nu(k,\tau) = \frac{4}{3}\delta_b(k,\tau) = \frac{4}{3}\delta_c(k,\tau) = -\frac{1}{3}k^2\tau^2\left(1 - \frac{\omega}{5}\tau\right), \tag{A4}$$

$$\theta_c(k,\tau) = 0, \tag{A5}$$

$$\theta_\gamma(k,\tau) = \theta_b(k,\tau) = -\frac{k^4\tau^3}{36}\left[1 - \frac{3}{20}\frac{F_i(1-R_\nu+5R_b) + 30\xi^2\sigma_i^2}{(1-R_\nu)F_i}\omega\tau\right], \tag{A6}$$

$$\theta_\nu(k,\tau) = -\frac{k^4\tau^3}{36}\left[\frac{23+4R_\nu}{15+4R_\nu} - \frac{3(275+50R_\nu+8R_\nu^2)F_i - 180(-5+4R_\nu)\xi^2\sigma_i^2}{20(15+2R_\nu)(15+4R_\nu)F_i}\omega\tau\right], \tag{A7}$$

$$\sigma_\nu(k,\tau) = \frac{2k^2\tau^2}{3(15+4R_\nu)}\left[1 + \frac{(-5+4R_\nu)(F+6\xi^2\sigma_i^2)}{4(15+2R_\nu)F_i}\omega\tau\right], \tag{A8}$$

$$\eta(k,\tau) = 1 - \frac{k^2\tau^2}{12}\left[\frac{5+4R_\nu}{15+4R_\nu} - \frac{150(-5+4R_\nu)\xi^2\sigma_i^2 + (325+280R_\nu+16R_\nu^2)F_i}{10(15+4R_\nu)(15+2R_\nu)F_i}\omega\tau\right], \tag{A9}$$

$$h(k,\tau) = \frac{k^2\tau^2}{2}\left(1 - \frac{\omega}{5}\tau\right), \tag{A10}$$

$$\delta\sigma(k,\tau) = -\frac{1}{8}k^2\tau^3\xi\omega\sigma_i\left[1 - \frac{2\xi^2\sigma_i^2(24+45\xi) + (4-9\xi)F_i}{10(F_i+6\xi^2\sigma_i^2)}\omega\tau\right], \tag{A11}$$

where $R_\nu = \frac{\rho_{\nu 0}}{\rho_r 0}$ and $R_b = \frac{\rho_{b0}}{\rho_{m0}}$.

[1] Jean-Philippe Uzan, "Varying Constants, Gravitation and Cosmology," Living Rev. Rel. **14**, 2 (2011), arXiv:1009.5514 [astro-ph.CO].

[2] P. A. R. Ade *et al.* (Planck), "Planck 2013 results. XVI. Cosmological parameters," Astron. Astrophys. **571**, A16 (2014), arXiv:1303.5076 [astro-ph.CO].

[3] C. Umiltà, M. Ballardini, F. Finelli, and D. Paoletti, "CMB and BAO constraints for an induced gravity dark energy model with a quartic potential," JCAP **1508**, 017 (2015), arXiv:1507.00718 [astro-ph.CO].

[4] Mario Ballardini, Fabio Finelli, Caterina Umiltà, and Daniela Paoletti, "Cosmological constraints on induced gravity dark energy models," JCAP **1605**, 067 (2016), arXiv:1601.03387 [astro-ph.CO].

[5] Pascual Jordan, "Formation of the Stars and Development of the Universe," Nature **164**, 637–640 (1949).

[6] C. Brans and R. H. Dicke, "Mach's principle and a relativistic theory of gravitation," Phys. Rev. **124**, 925–935 (1961).

[7] Xue-lei Chen and Marc Kamionkowski, "Cosmic microwave background temperature and polarization anisotropy in Brans-Dicke cosmology," Phys. Rev. **D60**,

104036 (1999), arXiv:astro-ph/9905368 [astro-ph].
[8] Ryo Nagata, Takeshi Chiba, and Naoshi Sugiyama, "WMAP constraints on scalar- tensor cosmology and the variation of the gravitational constant," Phys. Rev. **D69**, 083512 (2004), arXiv:astro-ph/0311274 [astro-ph].
[9] Viviana Acquaviva, Carlo Baccigalupi, Samuel M. Leach, Andrew R. Liddle, and Francesca Perrotta, "Structure formation constraints on the Jordan-Brans-Dicke theory," Phys. Rev. **D71**, 104025 (2005), arXiv:astro-ph/0412052 [astro-ph].
[10] A. Avilez and C. Skordis, "Cosmological constraints on Brans-Dicke theory," Phys. Rev. Lett. **113**, 011101 (2014), arXiv:1303.4330 [astro-ph.CO].
[11] Yi-Chao Li, Feng-Quan Wu, and Xuelei Chen, "Constraints on the Brans-Dicke gravity theory with the Planck data," Phys. Rev. **D88**, 084053 (2013), arXiv:1305.0055 [astro-ph.CO].
[12] Junpei Ooba, Kiyotomo Ichiki, Takeshi Chiba, and Naoshi Sugiyama, "Planck constraints on scalar-tensor cosmology and the variation of the gravitational constant," Phys. Rev. **D93**, 122002 (2016), arXiv:1602.00809 [astro-ph.CO].
[13] Gregory Walter Horndeski, "Second-order scalar-tensor field equations in a four-dimensional space," Int. J. Theor. Phys. **10**, 363–384 (1974).
[14] M. Ballardini, D. Sapone, C. Umiltà, F. Finelli, and D. Paoletti, "Testing extended Jordan-Brans-Dicke theories with future cosmological observations," (2019), arXiv:1902.01407 [astro-ph.CO].
[15] David Alonso, Emilio Bellini, Pedro G. Ferreira, and Miguel Zumalacárregui, "Observational future of cosmological scalar-tensor theories," Phys. Rev. **D95**, 063502 (2017), arXiv:1610.09290 [astro-ph.CO].
[16] Jean-Philippe Uzan, "Cosmological scaling solutions of nonminimally coupled scalar fields," Phys. Rev. **D59**, 123510 (1999), arXiv:gr-qc/9903004 [gr-qc].
[17] Francesca Perrotta, Carlo Baccigalupi, and Sabino Matarrese, "Extended quintessence," Phys. Rev. **D61**, 023507 (1999), arXiv:astro-ph/9906066 [astro-ph].
[18] Nicola Bartolo and Massimo Pietroni, "Scalar tensor gravity and quintessence," Phys. Rev. **D61**, 023518 (2000), arXiv:hep-ph/9908521 [hep-ph].
[19] Luca Amendola, "Scaling solutions in general nonminimal coupling theories," Phys. Rev. **D60**, 043501 (1999), arXiv:astro-ph/9904120 [astro-ph].
[20] Takeshi Chiba, "Quintessence, the gravitational constant, and gravity," Phys. Rev. **D60**, 083508 (1999), arXiv:gr-qc/9903094 [gr-qc].
[21] T. Baker, E. Bellini, P. G. Ferreira, M. Lagos, J. Noller, and I. Sawicki, "Strong constraints on cosmological gravity from GW170817 and GRB 170817A," Phys. Rev. Lett. **119**, 251301 (2017), arXiv:1710.06394 [astro-ph.CO].
[22] Paolo Creminelli and Filippo Vernizzi, "Dark Energy after GW170817 and GRB170817A," Phys. Rev. Lett. **119**, 251302 (2017), arXiv:1710.05877 [astro-ph.CO].
[23] Jose María Ezquiaga and Miguel Zumalacárregui, "Dark Energy After GW170817: Dead Ends and the Road Ahead," Phys. Rev. Lett. **119**, 251304 (2017), arXiv:1710.05901 [astro-ph.CO].
[24] B. P. Abbott *et al.* (LIGO scientific, Virgo), "GW170817: Observation of Gravitational Waves from a Binary Neutron Star Inspiral," Phys. Rev. Lett. **119**, 161101 (2017), arXiv:1710.05832 [gr-qc].
[25] Lucas Lombriser and Andy Taylor, "Breaking a Dark Degeneracy with Gravitational Waves," JCAP **1603**, 031 (2016), arXiv:1509.08458 [astro-ph.CO].
[26] Lucas Lombriser and Nelson A. Lima, "Challenges to Self-Acceleration in Modified Gravity from Gravitational Waves and Large-Scale Structure," Phys. Lett. **B765**, 382–385 (2017), arXiv:1602.07670 [astro-ph.CO].
[27] C. Wetterich, "Cosmology and the Fate of Dilatation Symmetry," Nucl. Phys. **B302**, 668–696 (1988).
[28] Fred Cooper and Giovanni Venturi, "Cosmology and Broken Scale Invariance," Phys. Rev. **D24**, 3338 (1981).
[29] F. Finelli, A. Tronconi, and Giovanni Venturi, "Dark Energy, Induced Gravity and Broken Scale Invariance," Phys. Lett. **B659**, 466–470 (2008), arXiv:0710.2741 [astro-ph].
[30] Fedor L. Bezrukov and Mikhail Shaposhnikov, "The Standard Model Higgs boson as the inflaton," Phys. Lett. **B659**, 703–706 (2008), arXiv:0710.3755 [hep-th].
[31] B. Boisseau, Gilles Esposito-Farese, D. Polarski, and Alexei A. Starobinsky, "Reconstruction of a scalar tensor theory of gravity in an accelerating universe," Phys. Rev. Lett. **85**, 2236 (2000), arXiv:gr-qc/0001066 [gr-qc].
[32] Radouane Gannouji, David Polarski, Andre Ranquet, and Alexei A. Starobinsky, "Scalar-Tensor Models of Normal and Phantom Dark Energy," JCAP **0609**, 016 (2006), arXiv:astro-ph/0606287 [astro-ph].
[33] Chung-Pei Ma and Edmund Bertschinger, "Cosmological perturbation theory in the synchronous and conformal Newtonian gauges," Astrophys. J. **455**, 7–25 (1995), arXiv:astro-ph/9506072 [astro-ph].
[34] Massimo Rossi, "Dark Energy as a scalar field nonminimally coupled to gravity," (2016).
[35] Alain Riazuelo and Jean-Philippe Uzan, "Quintessence and gravitational waves," Phys. Rev. **D62**, 083506 (2000), arXiv:astro-ph/0004156 [astro-ph].
[36] Luca Amendola, Guillermo Ballesteros, and Valeria Pettorino, "Effects of modified gravity on B-mode polarization," Phys. Rev. **D90**, 043009 (2014), arXiv:1405.7004 [astro-ph.CO].
[37] Andrew R. Liddle, Anupam Mazumdar, and John D. Barrow, "Radiation matter transition in Jordan-Brans-Dicke theory," Phys. Rev. **D58**, 027302 (1998), arXiv:astro-ph/9802133 [astro-ph].
[38] Y. Akrami *et al.* (Planck), "Planck 2018 results. X. Constraints on inflation," (2018), arXiv:1807.06211 [astro-ph.CO].
[39] P. A. R. Ade *et al.* (BICEP2, Keck Array), "BICEP2 / Keck Array x: Constraints on Primordial Gravitational Waves using Planck, WMAP, and New BICEP2/Keck Observations through the 2015 Season," Phys. Rev. Lett. **121**, 221301 (2018), arXiv:1810.05216 [astro-ph.CO].
[40] Benjamin Audren, Julien Lesgourgues, Karim Benabed, and Simon Prunet, "Conservative Constraints on Early Cosmology: an illustration of the Monte Python cosmological parameter inference code," JCAP **1302**, 001 (2013), arXiv:1210.7183 [astro-ph.CO].
[41] Thejs Brinckmann and Julien Lesgourgues, "MontePython 3: boosted MCMC sampler and other features," (2018), arXiv:1804.07261 [astro-ph.CO].
[42] Diego Blas, Julien Lesgourgues, and Thomas Tram, "The Cosmic Linear Anisotropy Solving System (CLASS) II: Approximation schemes," JCAP **1107**, 034 (2011), arXiv:1104.2933 [astro-ph.CO].
[43] N. Aghanim *et al.* (Planck), "Planck 2015 results.

XI. CMB power spectra, likelihoods, and robustness of parameters," Astron. Astrophys. **594**, A11 (2016), arXiv:1507.02704 [astro-ph.CO].

[44] P. A. R. Ade *et al.* (Planck), "Planck 2015 results. XV. Gravitational lensing," Astron. Astrophys. **594**, A15 (2016), arXiv:1502.01591 [astro-ph.CO].

[45] Florian Beutler, Chris Blake, Matthew Colless, D. Heath Jones, Lister Staveley-Smith, Lachlan Campbell, Quentin Parker, Will Saunders, and Fred Watson, "The 6dF Galaxy Survey: Baryon Acoustic Oscillations and the Local Hubble Constant," Mon. Not. Roy. Astron. Soc. **416**, 3017–3032 (2011), arXiv:1106.3366 [astro-ph.CO].

[46] Lauren Anderson *et al.* (BOSS), "The clustering of galaxies in the SDSS-III Baryon Oscillation Spectroscopic Survey: baryon acoustic oscillations in the Data Releases 10 and 11 Galaxy samples," Mon. Not. Roy. Astron. Soc. **441**, 24–62 (2014), arXiv:1312.4877 [astro-ph.CO].

[47] Ashley J. Ross, Lado Samushia, Cullan Howlett, Will J. Percival, Angela Burden, and Marc Manera, "The clustering of the SDSS DR7 main Galaxy sample – I. A 4 per cent distance measure at $z = 0.15$," Mon. Not. Roy. Astron. Soc. **449**, 835–847 (2015), arXiv:1409.3242 [astro-ph.CO].

[48] O. Pisanti, A. Cirillo, S. Esposito, F. Iocco, G. Mangano, G. Miele, and P. D. Serpico, "PArthENoPE: Public Algorithm Evaluating the Nucleosynthesis of Primordial Elements," Comput. Phys. Commun. **178**, 956–971 (2008), arXiv:0705.0290 [astro-ph].

[49] Jan Hamann, Julien Lesgourgues, and Gianpiero Mangano, "Using BBN in cosmological parameter extraction from CMB: A Forecast for PLANCK," JCAP **0803**, 004 (2008), arXiv:0712.2826 [astro-ph].

[50] P. A. R. Ade *et al.* (Planck), "Planck 2015 results. XIII. Cosmological parameters," Astron. Astrophys. **594**, A13 (2016), arXiv:1502.01589 [astro-ph.CO].

[51] Adam G. Riess *et al.*, "Milky Way Cepheid Standards for Measuring Cosmic Distances and Application to Gaia DR2: Implications for the Hubble Constant," Astrophys. J. **861**, 126 (2018), arXiv:1804.10655 [astro-ph.CO].

[52] Adam G. Riess *et al.*, "A 2.4% Determination of the Local Value of the Hubble Constant," Astrophys. J. **826**, 56 (2016), arXiv:1604.01424 [astro-ph.CO].

[53] Antonio J. Cuesta, Licia Verde, Adam Riess, and Raul Jimenez, "Calibrating the cosmic distance scale ladder: the role of the sound horizon scale and the local expansion rate as distance anchors," Mon. Not. Roy. Astron. Soc. **448**, 3463–3471 (2015), arXiv:1411.1094 [astro-ph.CO].

[54] Jose Luis Bernal, Licia Verde, and Adam G. Riess, "The trouble with H_0," JCAP **1610**, 019 (2016), arXiv:1607.05617 [astro-ph.CO].

[55] Kevin Aylor, MacKenzie Joy, Lloyd Knox, Marius Millea, Srinivasan Raghunathan, and W. L. Kimmy Wu, "Sounds Discordant: Classical Distance Ladder & ΛCDM -based Determinations of the Cosmological Sound Horizon," Astrophys. J. **874**, 4 (2019), arXiv:1811.00537 [astro-ph.CO].

[56] Vivian Poulin, Tristan L. Smith, Daniel Grin, Tanvi Karwal, and Marc Kamionkowski, "Cosmological implications of ultralight axionlike fields," Phys. Rev. **D98**, 083525 (2018), arXiv:1806.10608 [astro-ph.CO].

[57] Vivian Poulin, Tristan L. Smith, Tanvi Karwal, and Marc Kamionkowski, "Early Dark Energy Can Resolve The Hubble Tension," (2018), arXiv:1811.04083 [astro-ph.CO].

[58] Prateek Agrawal, Francis-Yan Cyr-Racine, David Pinner, and Lisa Randall, "Rock 'n' Roll Solutions to the Hubble Tension," (2019), arXiv:1904.01016 [astro-ph.CO].

[59] Clifford M. Will, "The Confrontation between General Relativity and Experiment," Living Rev. Rel. **17**, 4 (2014), arXiv:1403.7377 [gr-qc].

[60] B. Bertotti, L. Iess, and P. Tortora, "A test of general relativity using radio links with the Cassini spacecraft," Nature **425**, 374–376 (2003).

[61] C. Wetterich, "Cosmologies With Variable Newton's 'Constant'," Nucl. Phys. **B302**, 645–667 (1988).

[62] D. Paoletti, M. Braglia, F. Finelli, M. Ballardini, and C. Umiltà, "Isocurvature fluctuations in the effective Newton's constant," (2018), arXiv:1809.03201 [astro-ph.CO].

[63] Song Ming Du, "Scalar Stochastic Gravitational-Wave Background in Brans-Dicke Theory of Gravity," Phys. Rev. **D99**, 044057 (2019), arXiv:1812.06068 [gr-qc].

[64] B. P. Abbott *et al.* (LIGO Scientific, Virgo), "Tests of General Relativity with GW170817," (2018), arXiv:1811.00364 [gr-qc].

[65] Y. Akrami *et al.* (Planck), "Planck 2018 results. I. Overview and the cosmological legacy of Planck," (2018), arXiv:1807.06205 [astro-ph.CO].

[66] Y. Akrami *et al.* (Planck), "Planck 2018 results. II. Low Frequency Instrument data processing," (2018), arXiv:1807.06206 [astro-ph.CO].

[67] N. Aghanim *et al.* (Planck), "Planck 2018 results. III. High Frequency Instrument data processing and frequency maps," (2018), arXiv:1807.06207 [astro-ph.CO].